Bulletin of Engineering Geology and the Environment (2021) 80:5391–5403
https://doi.org/10.1007/s10064-021-02293-4

ORIGINAL PAPER

A massive ancient river-damming landslide triggered by buckling failure in the upper Jinsha River, SE Tibetan Plateau

Yanyan Li[1] · Xuyang Feng[1] · Aijun Yao[1] · Shan Lin[1] · Rui Wang[1] · Mingzhu Guo[1]

Received: 21 January 2021 / Accepted: 12 May 2021 / Published online: 18 May 2021

Abstract

Large-scale landsliding is an extremely important geological process in shaping landscapes in the Tibetan Plateau. In this research, an ancient river-damming landslide with an estimated debris volume of 4.9×10^7 m^3, located in the upper Jinsha River, SE Tibetan Plateau, was studied. The landslide once formed a dam over 60 m high and blocked the river. Lacustrine sediments, composed of silty clay with particle sizes of 0.002–0.25 mm, are intermittently distributed along both banks, extending about 6.5 km upstream. The OSL dating indicates that the lacustrine sediments have an age of 2.6 ± 0.2 ka. Detailed field investigation and theoretical analysis was performed to investigate the characteristics, potential cause and mechanism of the landslide. The results suggest that the landslide was most likely triggered by buckling of planar rock slabs under gravity. It may start as a translational sliding along the weak interlayer composed of mica schist at the upper part of the slope and then formed buckles by curving amphibolite rock beds near the slope toe. The hillslope has still been affected by gravitational deformations, with geomorphology characterized by tension cracks, buckle folds, and small landslide scars distributed on the slope surface, suggesting that the evolution of the river valley caused by buckling deformation has not achieved equilibrium.

Keywords Tibetan Plateau · Buckling · Landslide dam · Lacustrine sediments

Introduction

The geological environment in the Tibetan Plateau is one of the weakest environments in the world. This area has experienced complicated geological processes including uplift combined with fluvial or glacial downcutting, earthquakes, and precipitation, with the geomorphology characterized by steep hillslopes and deeply incised valleys (Deng et al. 2019). Large-scale landsliding is of great significance in shaping landscapes in the Tibetan Plateau (Dortch et al. 2009). Especially, massive landslide debris could rush into river valleys and form dammed lakes, causing catastrophic floods threatening to human life and property because of the breakage of the dams (Fan et al. 2014; Korup and Tweed 2007; Zhang et al. 2019). For example, the 2014 landslide disaster near Oso in Washington State, USA, caused more than 40 fatalities (Iverson et al. 2015), and the catastrophic Baige landslide occurring on October 10, 2018, in southwest China generated a dammed lake causing a direct economic loss of approximately 1.0 billion USD (Tian et al. 2020). Besides, records show that some of the largest floods on Earth were caused by the rapid release of water from landslide-dammed lakes (O'Connor and Costa 2004; Zhang et al. 2019; Fan et al. 2020).

To date, many large river-damming landslides have been mapped along the rivers in the Tibet Plateau (Wang et al. 2019; Wu et al. 2019, 2020), including Jinsha River (Chen et al. 2013; Kong et al. 2009; Li et al. 2020), Lancang River (Tu and Deng 2020), and Yarlung Tsangpo River (Liu et al. 2015). Among these landslides, the mechanism of ancient ones is particularly complicated. Earthquakes and heavy rainfall are deemed to be the most possible triggers for large-scale ancient river-damming landslides (Dortch et al. 2009). However, in alpine valleys of the Tibetan Plateau, catastrophic slope failure initiated by buckling deformations also plays an important role in shaping landscapes.

Buckling often develops in layered rock slopes where rock slabs are approximately parallel to the hillslope (Cavers 1981). Slab weight, pore water pressure, and earthquake all could be potential triggers of buckling (Zhao et al. 2018). Many methods are used to analyze the modes of buckling,

✉ Yanyan Li
lee_xandy@126.com

[1] Faculty of Urban Construction, Beijing University of Technology, Beijing 100124, China

such as the Euler's method, the limit equilibrium method, and numerical methods. Cavers (1981) developed a formula for different cases of buckling, including flexural buckling, three-hinge buckling of planar slopes and curved slopes. Tommasi et al. (2009) used the distinct element method to model buckling deformation of high natural slopes. Qi et al. (2015) proposed an analytical solution to analyze buckling failure caused by earthquake. Rosales Garzon (2016) used the tangent-modulus theory to study the mode of buckling failure. Zhao et al. (2018) analyzed the buckling mechanism of the Xinmo landslide using the Euler's method and found that the landslide was triggered by precipitation.

This paper reports a study of a large ancient river-damming landslide related to buckling failure in the Tibetan Plateau. Detailed field mapping and theoretical analysis was conducted to reveal the potential mechanism of the landslide. The failure of this landslide involves large buckles with different deformation phases, which provide a good chance to study the deformation mechanism of layered rock mass under relatively well-known boundary conditions.

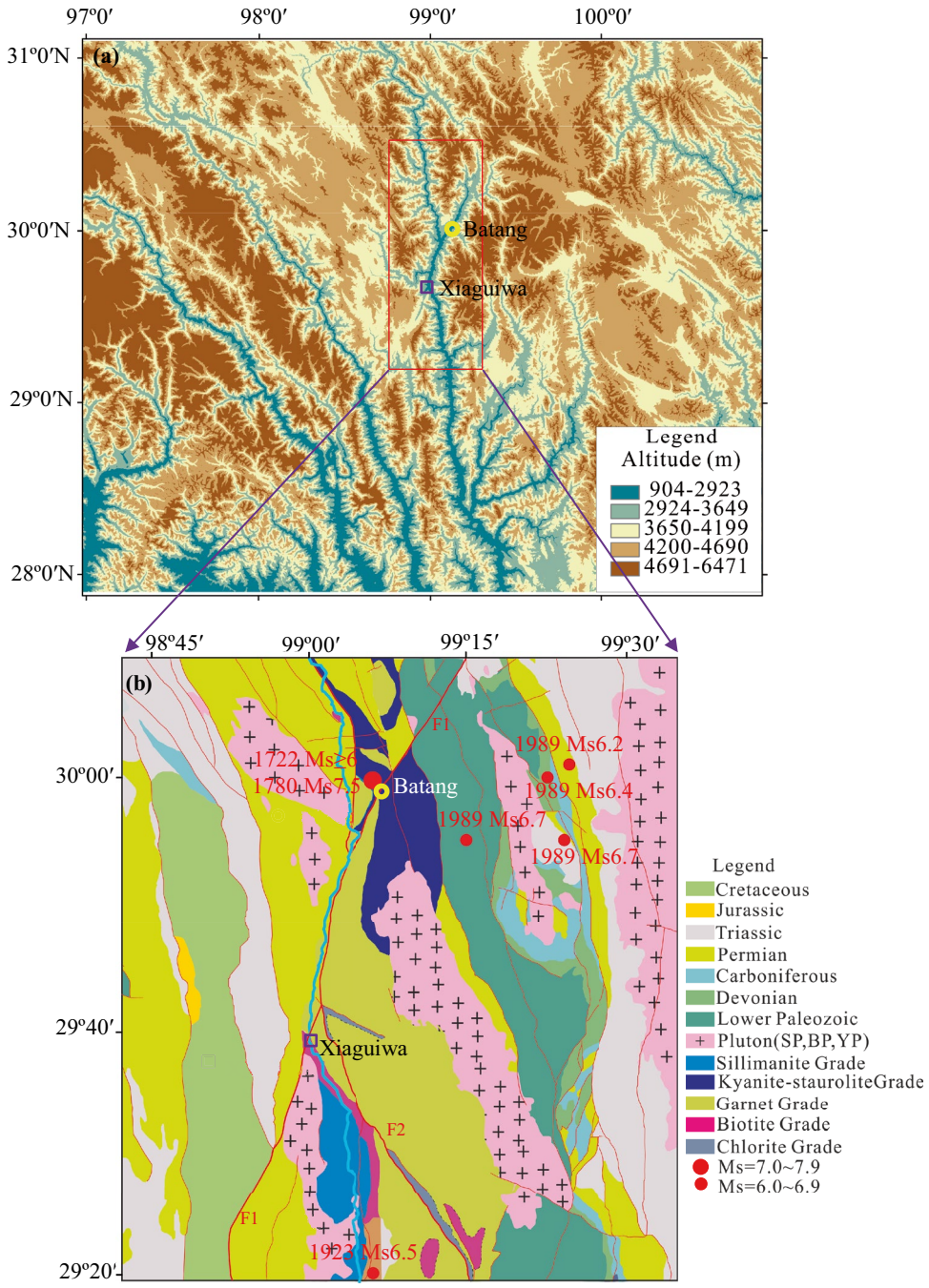

Fig. 1 Geomorphological and geological characteristics of the study area. (**a**) Topography. (**b**) Geological setting (modified from Cao et al. (2015))

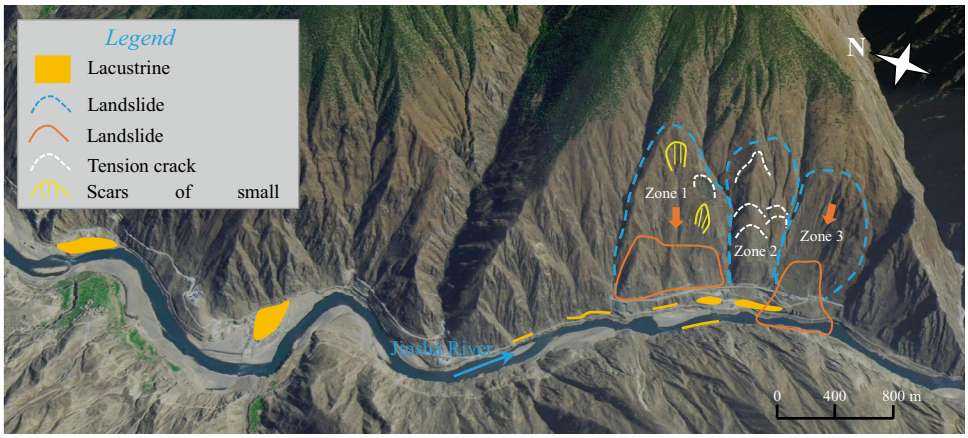

Fig. 2 Location of the Xiaguiwa landslide

Geological setting

The study area is located at the southeast fringe of the Tibetan Plateau, approximately 50 km to the south of the Batang county, Sichuan province (Fig. 1a). The geomorphology is characterized by steep hillslopes with slope angles varying from 30° to 65° and deeply incised valleys. Several large-scale ancient river-damming landslides have been mapped in this region (Chen et al. 2013; Li et al. 2020), which have strongly modified the landscape.

Rocks exposed in this region mainly consist of metamorphic rocks from the Lower Permian period, including mica schist, quartz schist, and amphibolite, which are highly fractured due to tectonic movement. Slope stability in this area is mainly affected by two regional faults (Fig. 1b): (1) the Batang fault (F1) and (2) the Xiongsong-Suwalong fault (F2). The Batang fault trends NE30° and is approximately 200 km long. It is a late Holocene active left-lateral strike-slip fault with the slip rate of 2–4 mm/year, which triggered the Batang earthquake (Ms 7.5) in 1870 (Huang et al. 2015). The Xiongsong-Suwalong fault, trending approximately SN with a length of 300 km, is a branch of the Jinshajiang fault belt which experienced a right-lateral strike-slip movement of hundreds of kilometers since the Paleocene (Bao et al. 2020). The Xiongsong-Suwalong fault is also a late Holocene active fault and triggered the Wangdalong earthquake

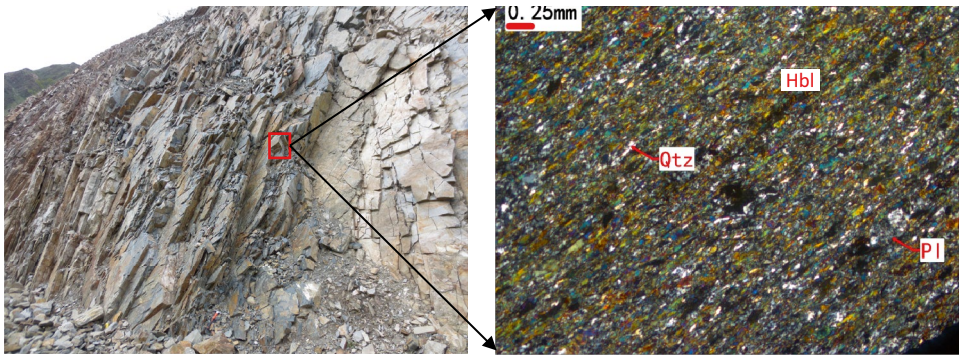

(a) Amphibolite and mineral composition

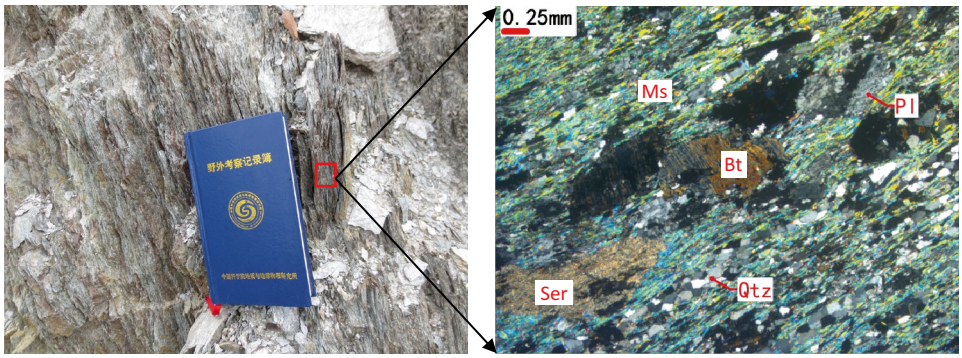

(b) Mica schist and mineral composition

Fig. 3 Rocks exposed in the study area and their mineral compositions. Abbreviations: Pl-plagioclase; Qtz-quartz; Hbl-hornblende; Bt-biotite; Ms-muscovite; Ser-sericite

(Ms 6.5) in 1923. Based on historical records of earthquake events (Wu and Cai 1992; Li et al. 2020), seven strong earthquakes (Ms ≥ 6) have occurred in the study area since 1722, as shown in Fig. 1b. Earthquakes cause strong ground vibrations (Castelli et al. 2021), alter the stress conditions in slopes, and generate discontinuities in bedrocks, which strongly affect landslide activity (Ferraro et al. 2009; Valagussa et al. 2019; Li et al. 2020).

This area has a semi-arid climate. The temperature ranges from − 10 °C in December–January to 35 °C in July–August. Rainfall is concentrated in June to September, and the average annual precipitation is 468.3 mm (Chen et al. 2013; Li et al. 2020). Vegetation in this area is poorly developed.

Characteristics of the Xiaguiwa landslide

Landslide description

The Xiaguiwa landslide is located at the east bank of the Jinsha River (Fig. 2). It covers a surface area of 1.7 km^2 with a width of 1000 m, a length of 1700 m and an estimated volume of 4.9×10^7 m^3. The elevation of the scarp is approximately 3200 m, and the elevation of the bottom of the source area is 2510 m which is 65 m above the river level (2445 m).

The valley of the Jinsha River in this region is formed by well stratified amphibolite with the interbed composed of mica schist, both in the Lower Permian age (Fig. 1b and Fig. 3). The polarized light microscopy based on thin sections was conducted for mineral identification (Zhu et al. 2011). The results show that the amphibolite mainly composed of hornblende (70 vol %), plagioclase (20%), and quartz (5%), developing a nematoblastic texture and a schistose structure. Besides, the mica schist mainly composed of muscovite (55 vol %), quartz (20%), plagioclase (10%), and biotite (10%), characterized by a lepidoblastic texture and a schistose structure. Field mapping shows that three sets of fractures are developed in the rock mass (Fig. 4): (1) fracture set 1 referring to bedding discontinuities with an average orientation of 245°∠41°, (2) fracture set 2 representing steeply dipping discontinuities with an average orientation of 169°∠78°, and (3) fracture set 3 with an average orientation of 51°∠40°. Bedding discontinuities are highly persistent, relatively planar and usually filled by clay or rock debris. They dip parallelly to the slope surface, with dip angles varying from 24° to 65°, divide amphibolite rocks into slabs (Fig. 3a), and thereby facilitate slope instability. Schist rocks are brittle and easy to be weathered, and the strength is sharply decreased when softened. Besides, the schist rock contains thin sericitization horizons parallel to bedding discontinuities, which are weaker than the bedding material (Fig. 3b).

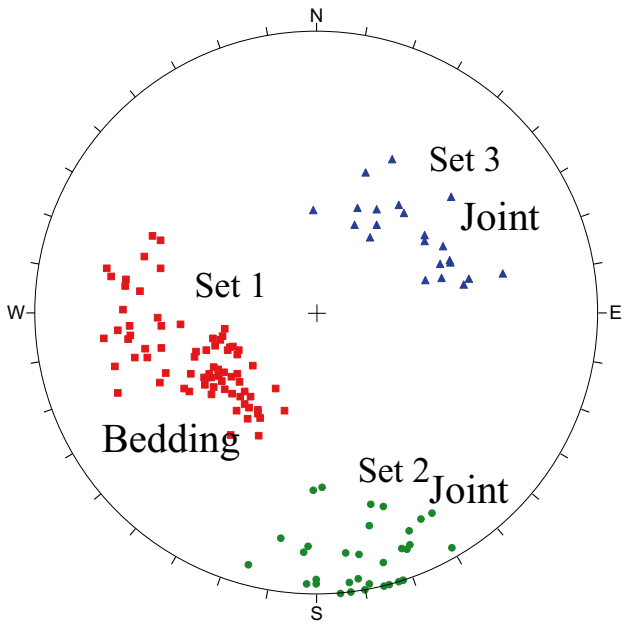

Fig. 4 Upper-hemisphere and equal-area projections of fracture orientations mapped from the studied rock slope. Set 1 refers to bedding discontinuities with an average orientation of 245°∠41°; set 2 refers to joints with an average orientation of 169°∠78°; set 3 refers to joints with an average orientation of 51°∠40°

Fig. 5 Characteristics of the slope in zone 1. (**a**) Geomorphology of zone 1. (**b**) Narrow platform in the middle of zone 1 caused by buckling. (**c**) Buckle fold exposed by excavation at the foot of zone 1. (**d**) Slip surface of the landslide and steeply dipping rock mass at the slope toe suffering from gravitational deformation. (**e**) Sketch map of profile I-I'

Detailed field investigations find that the Xiaguiwa landslide can be divided into 3 zones according to geomorphic features and deformation characteristics, as shown in Fig. 2. These zones are separated by small gullies. The upstream part of the landslide (zone 1) is characterized by planar rock surface, tension crack, buckle folds, and residual landslide debris overlaying on planar bedrocks. The downstream part of the landslide (zone 3) is characterized by steep head scarp, buckle folds, successive landslide deposits distributed below the scarp, and residual landslide dam in the river valley. In between (zone 2), the slope surface is strongly disturbed but without slope failure, characterized by a series of tension cracks trending parallelly to bedding discontinuities.

Zone 1

This zone is 0.8 km wide in the NW–SE direction and 1.0 km long (Fig. 5a). In the upper part of zone 1, bared bedrock is observed. There is a narrow platform with a width of about 5 m across the middle of this zone (Fig. 5b), which is assumed to be the hinge of a buckle fold. Below the platform, bared sliding surface is exposed, and three

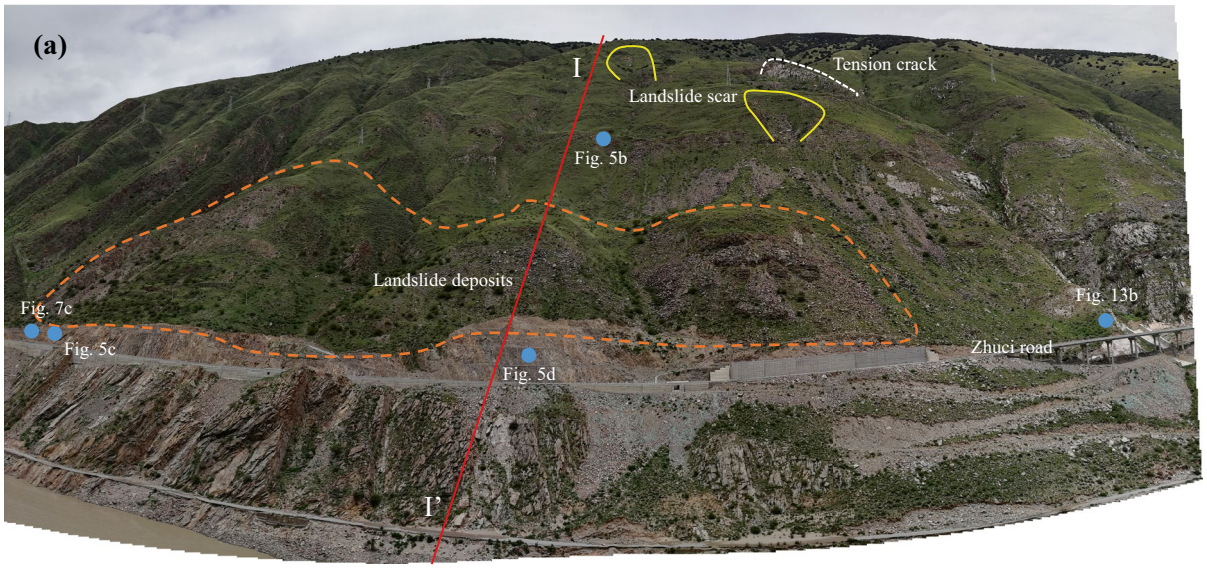
(a)
I
Tension crack
Landslide scar
Fig. 5b
Landslide deposits
Fig. 7c
Fig. 5c
Fig. 5d
Fig. 13b
Zhuci road
I'

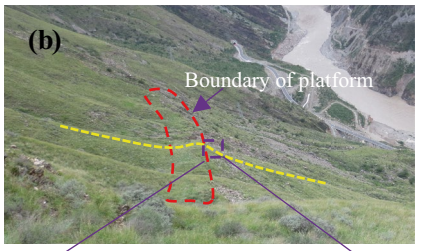
(b)
Boundary of platform

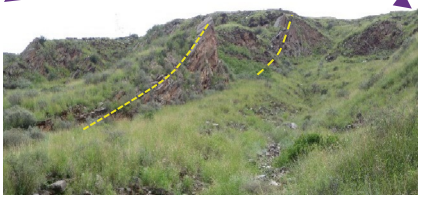


(c)

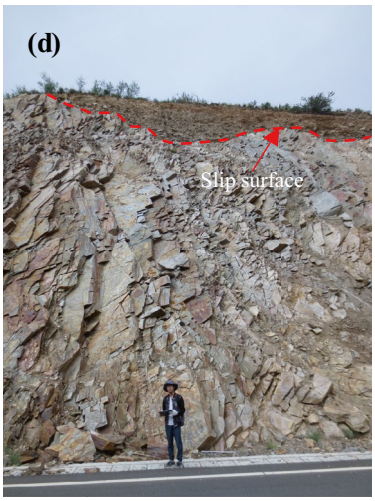
(d)
Slip surface

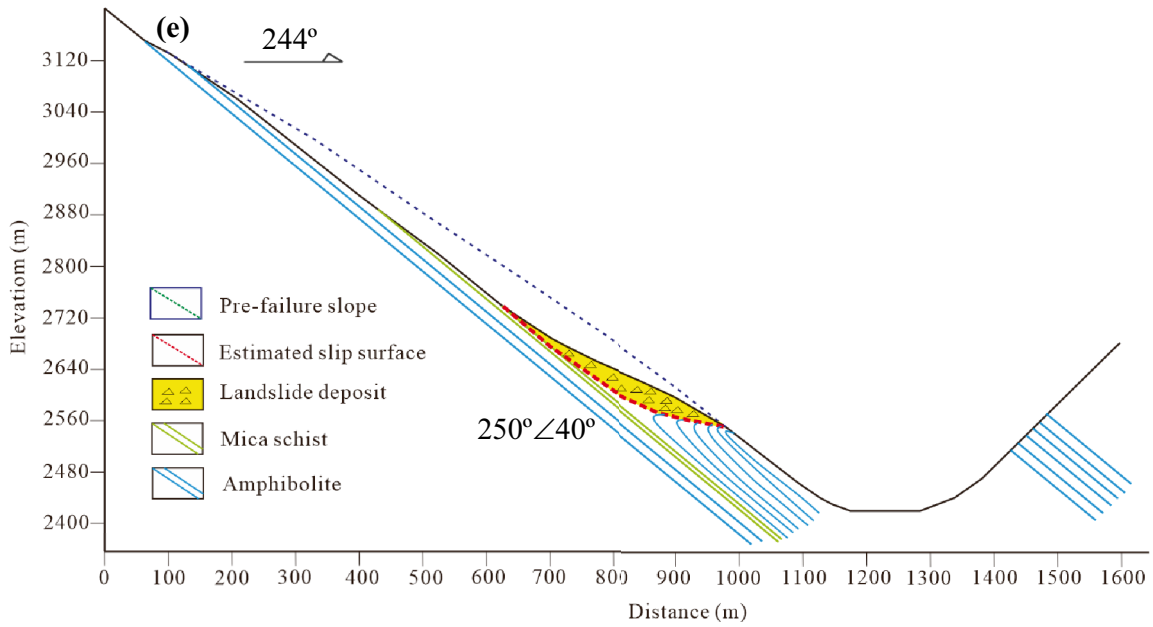
(e)
244°
3120
3040
2960
2880
2800
2720
2640
2560
2480
2400
Elevation (m)
Pre-failure slope
Estimated slip surface
Landslide deposit
Mica schist
Amphibolite
250°∠40°
0
100
200
300
400
500
600
700
800
900
1000
1100
1200
1300
1400
1500
1600
Distance (m)

separate rock avalanches are deposited at the elevation of 2510–2750 m (Fig. 5a). The ground surface created by the landslide above the Zhuci road is wrinkled by buckle folds (Fig. 5a,c). The rock mass near the toe of the slope has suffered from gravitational deformations, and the dip angle of the strata are steeper than elsewhere, reaching up to 70°, as shown in Fig. 5d. Below the Zhuci road, most of landslide deposits has been washed away by the river, only a small bit of deposits is distributed at the slope toe (Fig. 5a). As shown in Fig. 5e, a large portion of the slope is subjected to large displacements due to buckling. The exposed slide surface of the ancient landslide has been deformed by gravity after the main slide event. Two small shallow and bowl-shaped rockslide scars have been left above the platform (Fig. 5a).

Zone 2

Zone 2 is 0.4 km wide in the NW–SE direction and 0.8 km long. A series of tension cracks parallel to the bedding strike are exposed on the slope surface (Fig. 6a), indicating that the slope suffers from strongly polyphase gravitational deformations. Bedrocks outcrop around the extensional cracks, with the attitude of N30°W/45°SW (Fig. 6b). Field

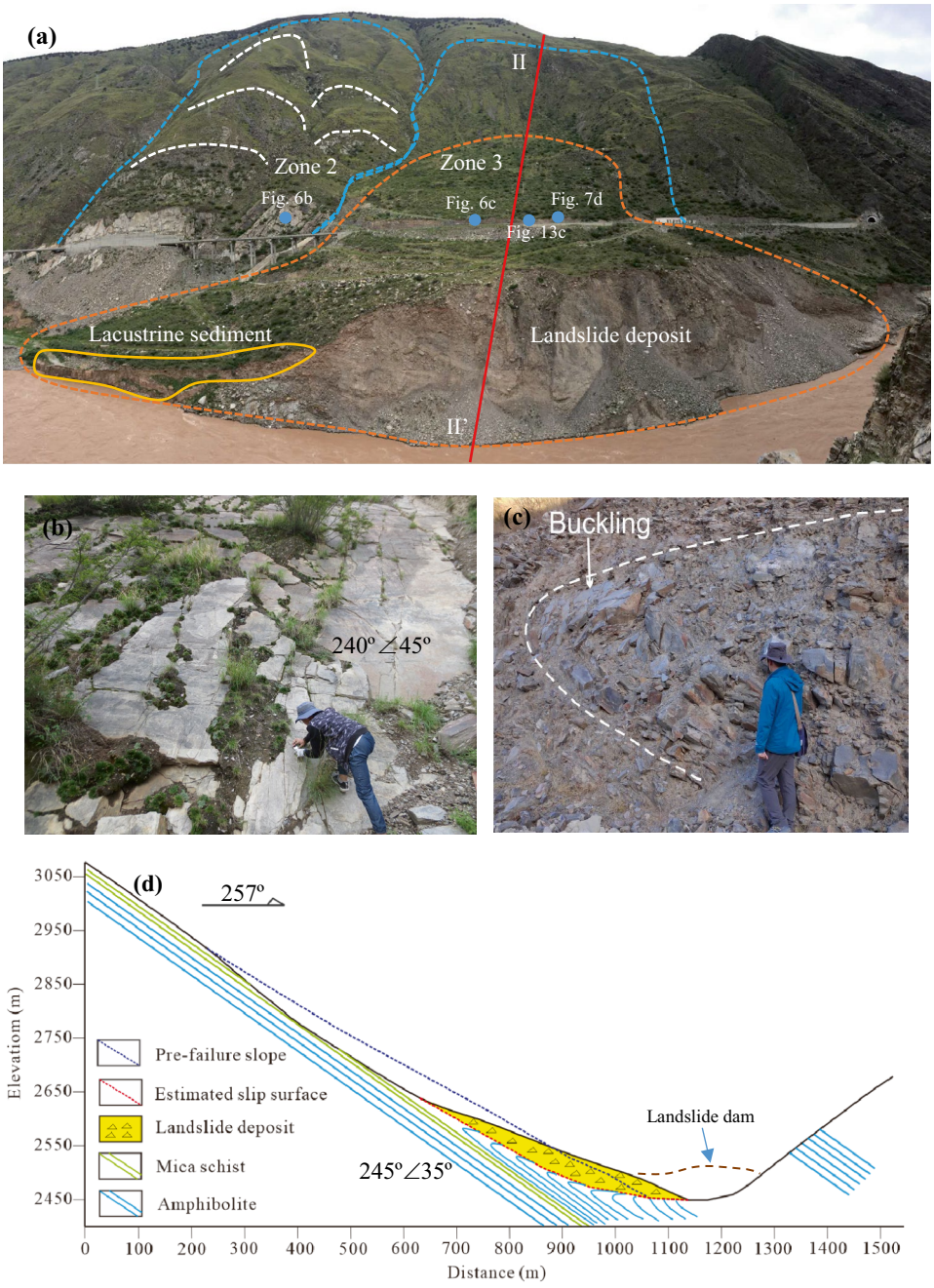

Fig. 6 Characteristics of the slope in zones 2 and 3. (**a**) Geomorphology of zones 2 and 3. (**b**) Bedrock exposed at the foot of zone 2. (**c**) Buckle fold exposed by excavation at the foot of zone 3. (**d**) Sketch map of profile II-II'

investigations show that the deformation of the slope in this zone has not reached equilibrium.

Zone 3

This region is 0.85 km long in the NE–SW direction and 0.5 km wide. The elevation of the top and the bottom of this landslide is 2970 m asl and 2510 m asl, respectively. Fan-like landslide deposits are distributed in the river valley at 2445–2520 m asl (Fig. 6a). The deposits once blocked the Jinsha River and formed a dammed lake. The height of the dam is estimated to be over 60 m based on the dam relic. Two successive deposits are observed (Fig. 6a): the landslide dam and a subsequent rockslide deposit overlying on the bedrock. Highway excavation cut through the toe of the landslide and a buckling fold was revealed (Fig. 6c), indicating the landslide is likely to be a toe buckling translational slide (Fig. 6d). Lacustrine sediments overlying on the landslide deposits are observed overlying on the landslide deposit (Fig. 6a). Optically stimulated luminescence (OSL) dating was performed on two samples obtained from the top of the lacustrine sediments in the front of the landslide dam (Fig. 6a). The samples were taken from freshly cleaned profiles using steel tubes. The OSL result shows that the landslide-dammed lake deposits at an age of 2.6 ± 0.2 ka.

Buckling deformations

The modes of buckling deformations can be grouped into two categories (Cavers 1981): three-hinge buckling and flexural buckling. The two kinds of buckling are observed in different regions of the study area in terms of the curvature and thickness of rock slabs.

Three-hinge buckling

Three-hinge buckling is observed at the upstream boundary of the Xiaguiwa landslide (Fig. 7a, b), as well as the platform in the middle part of zone 1 (Fig. 5b). Rock mass was cut into thin layers by a set of bedding discontinuities. The dip angle of bedding discontinuities progressively increases toward downhill, and the slope surface exhibits a gentle convex morphology (Fig. 7a). The pack of layers in three-hinge buckling is 3–5 m thick and the thickness of rock layers varies from 0.3 to 0.8 m.

Flexural buckling

Flexural buckling is distributed at the foot of zones 1 and 3, with elevations varying between 2510 and 2535 m, as shown in Fig. 7c, d. The pack of layers in flexural buckling is 10–30 m thick. Rock layers within flexural buckling are 0.1 to 0.5 m thick, which is thinner than those within three-hinge buckling. The axis of buckle fold induced by flexural buckling is approximately parallel to the strike of rock layers and normal to the sliding direction.

Characteristics of lacustrine sediments

When the Xiaguiwa landslide occurred, massive rock avalanche rushed into the Jinsha River, generated a landslide

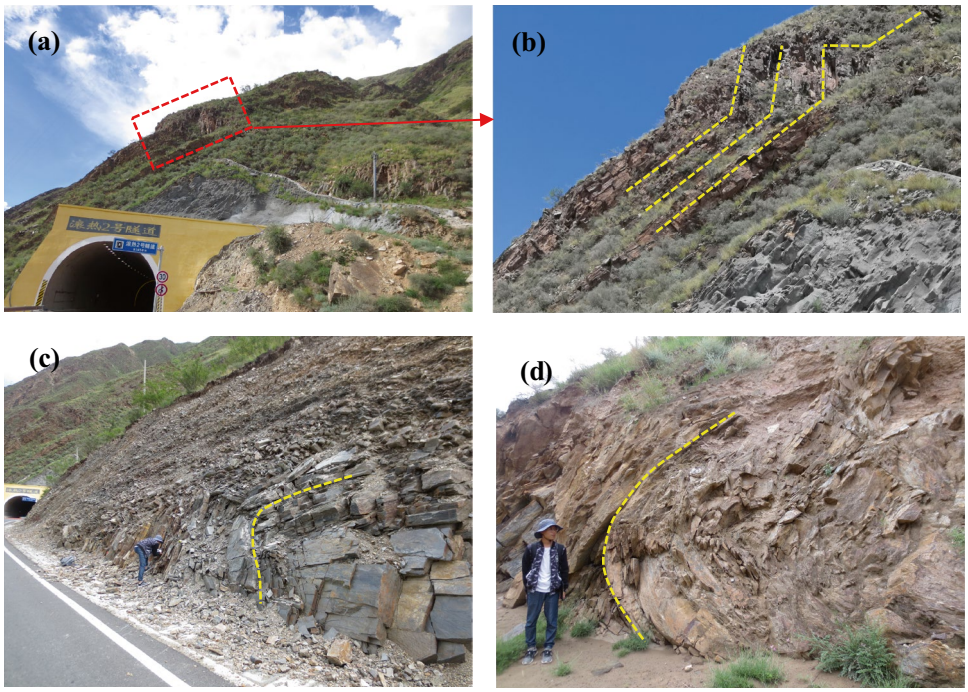

Fig. 7 Buckling deformations in the study area. (**a**) Three-hinge buckling at the upstream boundary of zone 1. (**b**) Photo showing the deformation of rock slabs in the threehinge buckling. (**c**) Flexural buckling at the foot of zone 1. (**d**) Flexural buckling near the foot of zone 3

dam over 60 m high below zone 3 and blocked the river (Fig. 6a). In the front of the dam, lacustrine sediments overly on landslide debris (Fig. 6a), indicating that they formed after the landslide. The lacustrine sediments are intermittently distributed along both banks, extending about 6.5 km upstream (Fig. 2). Characteristics of the lacustrine sediments caused by the Xiaguiwa landslide are shown in Fig. 8. The thickness of lacustrine sediments varies from 0.3 to 8 m. A special phenomenon was observed 1.8 km upstream from the landslide dam, as shown in Fig. 8d. Rock avalanche was buried by lacustrine sediments and appears as a locally phacoidal structure. We believe that three small landslides occurred in this area during the lacustrine sedimentation process. The debris of the landslides partially covered on the lacustrine deposits and afterwards was overlaid by subsequent sediments.

Particle gradation tests on two samples (samples 1 and 2) of lacustrine sediments were carried out. Note that sample 1 was obtained from the lacustrine sediments in the front of the landslide dam (Fig. 6a), and sample 2 was obtained from the lacustrine sediments 1.8 km upstream from the landslide dam (Fig. 8d).The results (Fig. 9) show that the lacustrine sediments are composed of silty clay with particle sizes of 0.002–0.25 mm, characterized by horizontally layered beddings (Fig. 8c), which is deemed to be typical lake sedimentary facies (Wu et al. 2019).

Fig. 8 Profiles of sediments in the study area along the Jinsha river. (**a**) Lacustrine sediments resting on rock avalanche. (**b**) Lacustrine sediments overlying on bedrock. (**c**) Lacustrine sediments with planar laminations. (**d**) Photo showing a lacustrine-colluvial depositional system. (**e**) Rhythmically bedded silty clay composed of regularly alternating light-yellow and gray laminae. (**f**) Rock avalanche appearing as a phacoidal structure

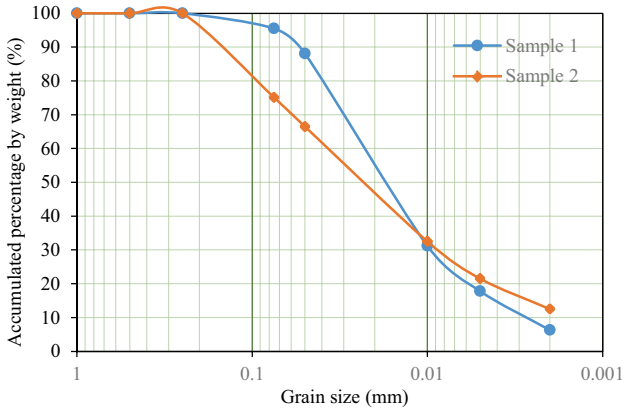

Fig. 9 Grain size distribution of lacustrine sediments. Samples 1 and 2 were obtained from the lacustrine sediments in the front of the landslide dam, and 1.8 km upstream from the landslide dam, respectively

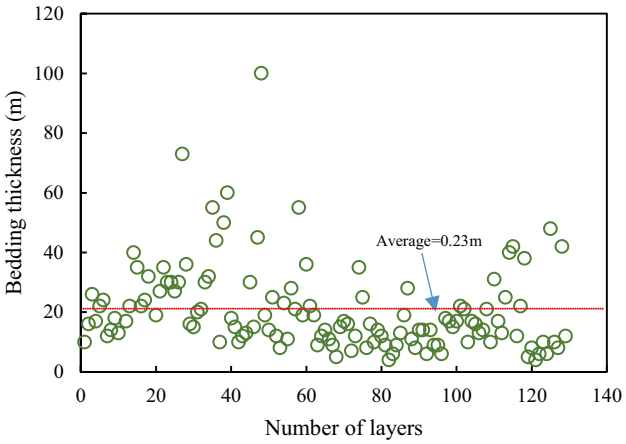

Fig. 10 Distribution of bedding thickness

Results and discussion

Generally, buckling mechanism requires that the dip of rock slabs is higher than the slope dip (Pereira and Lana 2012). The angle of internal friction, the slope dip and the discontinuity dip are controlling parameters for buckling deformations. Failure by buckling may be caused by the weight of the slab itself, by the increasing pore water pressure due to precipitation, by freezing pressures from ice, or by seismic shaking (Cavers 1981).

According to field investigations, rock formations in the study area are mainly composed of amphibolite in thin layers, characterized by crystalloblastic texture and schistose structure due to complicated tectonic activities. The amphibolite rocks are cut into planar slabs by bedding discontinuities that dip parallelly to the hillslope and have a steeper dip than the slope surface, which are prone to buckling. Thin-stratified mica schist outcrops as interlayers intercalated in the amphibolite formation, which is the weakest strata in the slope and provides a potential slip surface for the landslide. The environmental conditions including rainfall and seismic activities could be potential triggers for the Xiaguiwa landslide but are not well understood.

Table 1 Parameters used in the analysis

Property	Value
Bedding dip α (°) in profile I-I'	40
Total length L (m) in profile I-I'	450
Bedding dip α (°) in profile II-II'	35
Total length L (m) in profile II-II'	405
Unit weight (g/cm^3)	2.7
Cohesion (kPa)	0
Friction angle φ (°)	29
Young's modulus E (GPa)	9.1
Poison's ratio	0.25

Potential mechanism of buckling

In this work, the Euler formula (Cavers 1981) is used to analyze the potential mechanism of buckling deformations in the study area. In the method, the critical loading P_{cr} for buckling without considering pore water pressure is calculated by (Hu and Cruden 1993)

$$P_{cr} = \frac{\pi^2 EI}{4{L_b}^2} \tag{1}$$

where E refers to the Young's modulus, L_b means buckle length, and I is the moment of inertia computed by

$$I = \frac{t^3}{12} \tag{2}$$

where t refers to the thickness of buckled rock beds. The buckle force P_d caused by the weight of the upper portion of the rock beds is computed by (Hu and Cruden 1993)

$$P_d = \left(L - L_b\right)t(\gamma \sin\alpha - \gamma \cos\alpha \tan\varphi - c/t) \tag{3}$$

where L, α, and γ are the total length, the dip and the unit weight of a rock bed, respectively; φ and c are the internal friction angle and cohesion along the bedding discontinuity, respectively. The factor of safety F is defined as (Hu and Cruden 1993)

$$F = \frac{\pi^2 EI}{4{L_b}^2\left(L - L_b\right)\, t\,(\gamma \sin\alpha - \gamma \cos\alpha \tan\varphi - c/t)} \tag{4}$$

Then

$$\frac{\partial F}{\partial L_b} = \frac{\pi^2 EI\left[2L_b\left(L-L_b\right)-{L_b}^2\right]}{4{L_b}^4\left(L-L_b\right)^2 t\left(\gamma \sin\alpha - \gamma\cos\alpha\tan\varphi - c/t\right)} \tag{5}$$

Solving Eq. $4=0$ gives $L_b=2L/3$, suggesting that F achieves minimum when $L_b=2L/3$. Assuming $F=1$, the critical slope length for buckling L_{cr} can be determined:

$$L_{cr} = 0.25\left(\frac{9\pi^2 Et^2}{\left(\gamma \sin\alpha - \gamma\cos\alpha\tan\varphi - c/t\right)}\right)^{1/3} \tag{6}$$

Parameters used for calculation are obtained from previous studies (Duan 2009; Du 2015) in the study area (Table 1). Field investigations show that the thickness of rock beds ranges from 0.04 to 1.00 m, with an average of 0.23 m, as shown in Fig. 10. The calculated results (Fig. 11a) show that the critical length of rock beds L_{cr} in profile I-I' varies from 32 to 278 m corresponding to the bed thickness ranging from 0.04 to 1.00 m, both smaller than the actual length of rock beds (450 m). Therefore, rock beds are long enough to buckle under self-weight. Besides, the length of rock beds in profile II-II' (405 m) is also longer than the critical length for buckling (40 to 340 m), suggesting that the rock bed in profile II-II' can buckle under gravity.

Assuming c is equal to zero, the relationship between buckle length L_b and bed thickness d under the critical state ($F=1$) is represented by

$$d = \frac{4L_b}{\pi}\left(\frac{3\gamma\left(L-L_b\right)\left(\sin\alpha - \cos\alpha\tan\varphi\right)}{E}\right)^{1/2} \tag{7}$$

This relation can be delineated by Fig. 11b. The maximum thickness of rock beds for buckling in profiles I-I' and II-II' is 2.06 m and 1.30 m, respectively. Since the bed thickness of the slope in the study area varies between 0.04 and 1.00 m, which is smaller than the maximum bed thickness for buckling, we could conclude that the rock beds are thin enough to buckle under self-weight.

Potential causes of slope failure

The study area experienced complicated geological processes including uplift combined with fluvial undercutting,

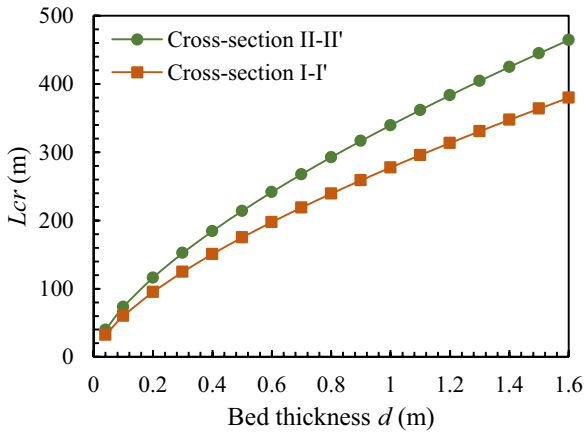

(a) Variation of L_{cr} with the thickness of rock beds

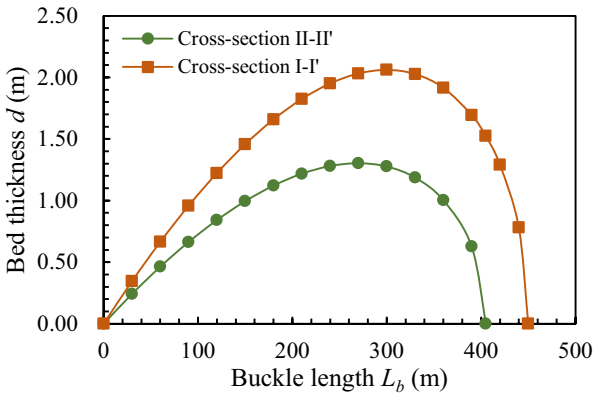

(b) Relationship between buckle length and bed thickness in the critical state

Fig. 11 Buckling analysis using the Euler's method

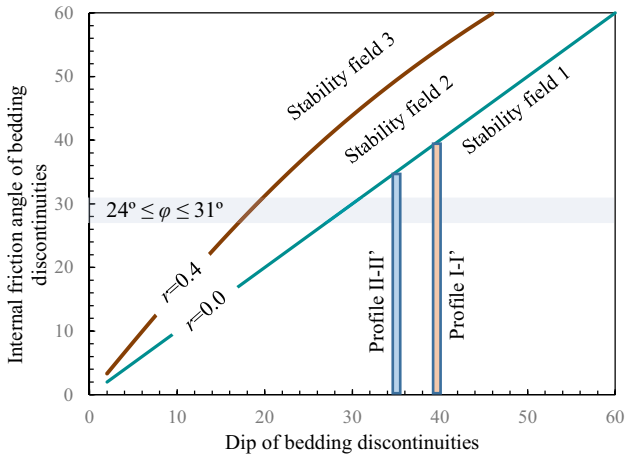

Fig. 12 The Xiaguiwa landslide plotted on idealized stability fields (modified from Dortch et al. (2009))

earthquakes, and rainfall. Therefore, determination of ancient landslide triggers in this area is difficult. The most likely triggers of landslides for a dip rock slope include rock mass properties, pore water pressure and earthquakes (Costa and Schuster 1988; Barnard et al. 2001; Cavallaro et al. 2019; Dortch et al. 2009; Tu and Deng 2020).

The information about pore water pressure and possible earthquakes when the Xiaguiwa landslide occurred, however, is unknown. In this work, a highly idealized sliding block model is used to analyze the possible causes of the landslide. The factor of safety F for a dip slope can be calculated by (Dortch et al. 2009).

$$F = (1 - r)\frac{\tan\varphi}{\tan\beta} \tag{8}$$

where r represents the coefficient of pore- or cleft-water pressure coefficient; β and φ refer to the dip and the internal friction angle of the potential sliding surface, respectively. Cohesion along the sliding surface is assumed to be zero. The value of r ranges from 0 to 0.4 for non-artesian conditions, while the value of φ generally changes between 25° and 45°, relying on the characteristic of discontinuities and lithology (Dortch et al. 2009). Therefore, three stability fields can be defined for a slope, as shown in Fig. 12: (1) slopes falling within stability field 1 are unconditionally

Fig. 13 Mica schist outcrops in the slope. (**a**) Mica schist below the platform of zone 1. (**b**) Mica schist distributed on the slip surface at the downstream boundary of zone 1. (**c**) Landslide deposits composed of mica schist exposed near the toe of zone 3

unstable; (2) slopes falling within stability field 2 will fail due to the increase of pore-water pressure; and (3) slopes falling within stability field 3 needs additional forces such as earthquakes to fail.

The internal friction angles along the beddings of mica schist vary from 24° and 31° (Wang 2014). The dip of rock beds in profiles I-I' and II-II' are 40° and 35°, respectively. Thus, the slope in zones 1 and 2 is completely plotted within stability field 1 (Fig. 12), indicating that it can fail by buckling just under gravity. Based on the idealized model, we could conclude that the Xiaguiwa landslide was likely to start as gravitationally induced buckling of rock slabs, which agrees well with the results obtained by the Euler's formula. More specifically, the landslide may initiate as a translational sliding along the weak interlayer composed of mica schist at the upper part of the slope and then formed buckles by curving amphibolite rock beds near the slope toe. This conclusion is supported by field investigations: (1) residual mica schist with a thickness of 1.2 m, which is strongly weathered, outcrops below the platform of zone 1 (Fig. 13a), which is deemed to be an ideal slip surface for the landslide; (2) strongly weathered mica schist is exposed on the slip surface at the downstream boundary of zone 1(Fig. 13b); and (3) landslide deposits composed of mica schist is exposed by road excavation near the toe of zone 3 (Fig. 13c).

Earthquake or pore water pressure, however, cannot be excluded as a potential trigger for the Xiaguiwa landslide. Affected by the two late Holocene active faults, the Xiongsong-Suwanglong fault and the Batang fault, the study area has experienced several strong earthquakes ($Ms \geq 6$) on centennial to millennial timescales. These earthquakes are responsible for many landslides in the Batang-Suwalong segment of the Jinsha River (Chen et al. 2013; Li et al. 2020). Field investigation shows that the mica schist interbed and rock mass structure are responsible for the slope instability. Toe erosion caused by rapid and continuous downcutting of the Jinsha River forces layered rock mass to intensively buckle. The slope surface after the landslide has been deformed by gravitational deformations, characterized by small landslide scars, tension cracks and buckle folds (Fig. 5 and Fig. 6). Therefore, the evolution of the river valley caused by large-scale landsliding has not achieved equilibrium.

Conclusions

This paper reports a study of a large ancient river-damming landslide related to buckling failure in the Tibetan Plateau. The landslide with an estimated debris volume of 4.9×10^7 m^3 is located at the upper Jinsha River, SE Tibetan Plateau. It once formed a landslide dam over 60 m high and blocked the river. Lacustrine sediments, composed of silty clay with particle sizes of 0.002–0.25 mm, are intermittently distributed along both banks, extending about 6.5 km upstream. The OSL dating indicates that the lacustrine sediments have an age of 2.6 ± 0.2 ka. Field investigation shows that the landslide can be divided into three zones based on geomorphic features, and each zone has different characteristics that provide information on the mechanism of the landslide.

Theoretical analysis was performed to investigate the potential cause and mechanism of the landslide. The results suggest that the river-damming landslide is most likely triggered by buckling of planar rock slabs induced by gravity. The intercalation of mica schist interbeds in the amphibolite formation and the structural conditions are responsible for the slope instability. The landslide may start as a translational sliding along the weak interlayer composed of mica schist at the upper part of the slope and then formed buckles by curving amphibolite rock beds near the slope toe. Earthquake or pore water pressure, however, cannot be excluded as a potential trigger for the slope failure, given that the study area is in a seismically active zone and suffers from heavy precipitation during the rainy season. The hillslope has still been affected by deformational deformations, characterized by tension cracks, buckle folds, and small landslide scars distributed on the slope surface, suggesting that the evolution of the river valley caused by large-scale landsliding has not achieved equilibrium.

Funding This work was financially supported by the National Key Research and Development Project of China (Nos. 2018YFC1505001 and 2019YFC1509702).

References

Bao XS, Yang LQ, Gao X, Groves D, He WY, Li MM (2020) Geochemical discrimination between fertile and barren Eocene potassic porphyries in the Jinshajiang Cu–Au–Mo metallogenic belt SW China: Implications for petrogenesis and metallogeny. Ore Geol Rev 116:57–73

Barnard PL, Owen LA, Sharma MC, Finkel RC (2001) Natural and human induced landsliding in the Garhwal Himalaya of Northern India. Geomorphology 40:21–35

Cao W, Yan DP, Qiu L, Zhang Y, Qiu J (2015) Structural style and metamorphic conditions of the Jinshajiang metamorphic belt: Nature of the Paleo-Jinshajiang orogenic belt in the eastern Tibetan Plateau. J Asian Earth Sci 113:748–765

Castelli F, Grasso S, Lentini V, Sammito MSV (2021) Effects of soil-foundation-interaction on the seismic response of a cooling tower by 3D-FEM analysis. Geosciences 11:200

Cavallaro A, Abate G, Ferraro A, Giannone A, Grasso S (2019) Seismic slope stability analysis of rainfall-induced landslides in Sicily (Italy). In: The 7th International Conference on Earthquake Geotechnical Engineering, Rome, pp 1672–1680

Cavers D (1981) Simple methods to analyze buckling of rock slopes. Rock Mech 14(02):87–104

Chen J, Dai F, Lv T, Cui Z (2013) Holocene landslide-dammed lake deposits in the Upper Jinsha River, SE Tibetan Plateau and their ages. Quat Int 298:107–113

Costa JE, Schuster RL (1988) The formation and failure of nature dams. Geol Soc Am Bull 100:1054–1068

Deng JH, Dai FC, Wen BP, Yao X (2019) Investigation on the catastrophic mechanism and risk control measures of major landslides in Tibetan Plateau. Advanced Engineering Sciences 51(05):1–8 (**in Chinese**)

Dortch JM, Owen LA, Haneberg WC, Caffee MW, Dietsch C, Kamp U (2009) Nature and timing of large landslides in the Himalaya and Transhimalaya of northern India. Quat Sci Rev 28:1037–1054

Du, (2015) The study of slope stability of the right lower dam of Jinsha river Batang hydropower station. Chengdu University of Technology, Thesis (**in Chinese**)

Duan, (2009) Engineering geology study of the Batang hydropower station for selection of dam site. Lanzhou University, Thesis (**in Chinese**)

Fan X, Rossiter DG, van Westen CJ, Xu Q, Görüm T (2014) Empirical prediction of coseismic landslide dam formation. Earth Surf Process Landf 39(14):1913–1926

Fan X, Dufresne A, Siva Subramanian S, Strom A, Hermanns R, Tacconi Stefanelli C, Hewitt K, Yunus AP, Dunning S, Capra L, Geertsema M, Miller B, Casagli N, Jansen JD, Xu Q (2020) The formation and impact of landslide dams – State of the art. Earth Sci Rev 203:103–116

Ferraro A, Grasso S, Maugeri M (2009) Seismic vulnerability of a slope in central Italy. Wit Transactions on the Built Environment 110:345–355

Hu XQ, Cruden DM (1993) Buckling deformation in the Highwood Pass, Alberta. Can Geotech J 30:276–286

Huang X, Du Y, He Z, Ma B, Xie F (2015) Late Quaternary slip rate of the Batang Fault and its strain partitioning role in Yushu area, central Tibet. Tectonophysics 653:52–67

Iverson RM, George DL, Allstadt K, Reid ME, Collins BD, Vallance JW, Schilling SP, Godt JW, Cannon CM, Magirl CS, Baum RL, Coe JA, Schulz WH, Bower JB (2015) Landslide mobility and hazards: implications of the 2014 Oso disaster. Earth Planet Sci Lett 412:197–208

Kong P, Na C, Fink D, Zhao X, Xiao W (2009) Moraine dam related to late Quaternary glaciation in the Yulong Mountains, southwest China, and impacts on the Jinsha River. Quat Sci Rev 28:3224–3235

Korup O, Tweed F (2007) Ice moraine and landslide dams in mountainous terrain. Quat Sci Rev 26:3406–3422

Li Y, Chen J, Zhou F, Song S, Zhang Y, Gu F, Cao C (2020) Identification of ancient river-blocking events and analysis of the mechanisms for the formation of landslide dams in the Suwalong section of the upper Jinsha River. SE Tibetan Plateau Geomorphology 368:107351

Liu W, La Z, Hu K, Ge Y, Cui P, Zhang X, Liu F (2015) Age and extent of a giant glacial-dammed lake at Yarlung Tsangpo gorge in the Tibetan Plateau. Geomorphology 246:370–376

O'Connor JE, Costa JE (2004) The world's largest floods, past and present-their causes and magnitudes, 1254. U.S. Geological Survey

Pereira LC, Lana MS (2012) Stress-strain analysis of buckling failure in phyllite slopes. Geotech Geol Eng 31:297–314

Qi S, Lan H, Dong J (2015) An analytical solution to slip buckling slope failure triggered by earthquake. Eng Geol 194:4–11

Rosales Garzon SE (2016) Analytical solution for assessing continuum buckling in sedimentary rock slopes based on the tangent-modulus theory. Int J Rock Mech Min Sci 90:53–61

Tian S, Chen N, Wu H, Yang C, Zhong Z, Rahman M (2020) New insights into the occurrence of the Baige landslide along the Jinsha River in Tibet. Landslides 17(05):1207–1216

Tommasi P, Verrucci L, Campedel P, Veronese L, Pettinelli E, Ribacchi R (2009) Buckling of high natural slopes: the case of Lavini di Marco (Trento-Italy). Eng Geol 109:93–108

Tu G, Deng H (2020) Formation and evolution of a successive landslide dam by the erosion of river: a case study of the Gendakan landslide dam on the Lancang River. China Bull Eng Geol Environ 79(06):2747–2761

Valagussa A, Marc O, Frattini P, Crosta GB (2019) Seismic and geological controls on earthquake-induced landslide size. Earth Planet Sci Lett 506:268–281

Wang JX (2014) Research for the anisotropy of quartz mica schist and its effect on the stability of the surrounding rock. Chengdu University of Technology, Thesis (**in Chinese**)

Wang H, Cui P, Liu D, Liu W, Bazai NA, Wang J, Zhang G, Lei Y (2019) Evolution of a landslide-dammed lake on the southeastern Tibetan Plateau and its influence on river longitudinal profiles. Geomorphology 343:15–32

Wu LZ, Deng H, Huang RQ, Zhang LM, Guo XG, Zhou Y (2019) Evolution of lakes created by landslide dams and the role of dam erosion: A case study of the Jiajun landslide on the Dadu River, China. Quat Int 503:41–50

Wu LZ, Zhao DJ, Zhu JD, Peng JB, Zhou Y (2020) A Late Pleistocene river-damming landslide, Minjiang River. China Landslides 17(02):433–444

Wu XG, Cai CX (1992) The neotectonic activity along the central segment of Jinshajiang Fault zone and the epicentral determination of Batang M6.5 earthquake. J Seismol Res 15:401–410 (**in Chinese**)

Zhang Y, Huang CC, Shulmeister J, Guo Y, Liu T, Kemp J, Patton NR, Liu L, Chen Y, Zhou Q, Cuan Y, Zhao H, Wang N (2019) Formation and evolution of the Holocene massive landslide-dammed lakes in the Jishixia Gorges along the upper Yellow River: No relation to China's Great Flood and the Xia Dynasty. Quat Sci Rev 218:267–280

Zhao S, Chigira M, Wu X (2018) Buckling deformations at the 2017 Xinmo landslide site and nearby slopes Maoxian Sichuan China. Eng Geol 246:187–197

Zhu JJ, Hu RZ, Bi XW, Zhong H, Chen H (2011) Zircon U-Pb ages, Hf-O isotopes and whole-rock Sr–Nd–Pb isotopic geochemistry of granitoids in the Jinshajiang suture zone SW China: Constraints on petrogenesis and tectonic evolution of the Paleo-Tethys Ocean. Lithos 126(03–04):248–264